EXPERIMENTAL AND NUMERICAL ANALYSIS OF WIND TURBINE MODEL

Biluš I. PhD.[1], Lešnik L. PhD.[1]
University of Maribor, Faculty of Mechanical Engineering, Slovenia [1]
ignacijo.bilus@um.si

Abstract: *Global demand for electric energy is predicted to increase in the coming decades. Following this, different approaches for additional electricity production are analysed and tested worldwide. The EU supports the production and usage of electricity from renewable energy sources, particularly wind energy, because it provides electricity without giving rise to any carbon dioxide emissions. The presented work analysis the possibility for utilising of wind-generated electricity as a stand-alone system for small off grid cabin supply. The very basic turbine geometry was designed and numerically simulated with commercial CFD software. After that, the turbine model was printed using 3D printer and tested in laboratory environment. The comparison of numerically and experimentally obtained operating characteristics show reasonable agreement and strong potential for system optimisation and improvements.*

Keywords: wind turbine, CFD, experiment

1. Introduction

To obtain wind power, the kinetic energy of wind is used to create mechanical power which is converted into electricity with generator. This makes the wind as unlimited, free, renewable energy resource with high economic value and low maintenance cost. The wind turbines harmlessly generate electricity from wind passing by. Wind energy is far more ecofriendly than the burning of fossil fuels for electricity production. On the other side, the wind energy has disadvantages as well. The two major disadvantages of wind power include initial cost and technology immaturity.

Firstly, constructing turbines and wind facilities is extremely expensive. The second disadvantage is technology immaturity, which predominantly address the current technology limits for offshore machines to shallow-water sites at a cost premium. New technology is needed to lower costs, increase reliability and energy production, expand the resource area and mitigate known environmental impacts [1].

The land based wind turbine technology researches, on the other side, addresses performance and reliability issues that wind power plants experience throughout their life span and reduces system costs through innovative technology development. Present study, address the solution simplicity on the case of small off grid wind power system. It was assumed, that area that have adequate wind, is available. Therefore, the analysis started with search for a suitable turbine geometry solution.

2. Wind turbine geometry

To determine the optimal wind turbine geometry, it is necessary to select or define some parameters and quantities as speed, Reynolds number, profile type and its span wise angle/length distribution. The outer diameter limit was set to d_{max}<300 mm according to the inner diameter of test section.

According to the diagram shown at Fig. 1 we selected the SG6043 profile. The complete geometry of turbine blades was defined using Betz and Schmitz's theory which provide the equations for the length of the blade profile and its angle distribution depending on the radius as follows [2].

Betz theory:

$$c_{Betz}(r) \approx 2\pi R \frac{1}{z} \frac{8}{9c_L} \frac{1}{\lambda_D^2 \left(\frac{r}{R}\right)}$$

$$\beta_{Betz} = arctan\left(\frac{2}{3}\frac{R}{r\lambda_D}\right) - \alpha_A$$

Schmitz theory:

$$c_{Schmitz}(r) = \frac{1}{z}\frac{16\,\pi\, r}{c_L}\sin\left(\frac{1}{3}\,\varphi_1\right)$$

$$\beta_{Schmitz} = atan\left(\frac{R}{r\lambda_D}\right) - \alpha_A$$

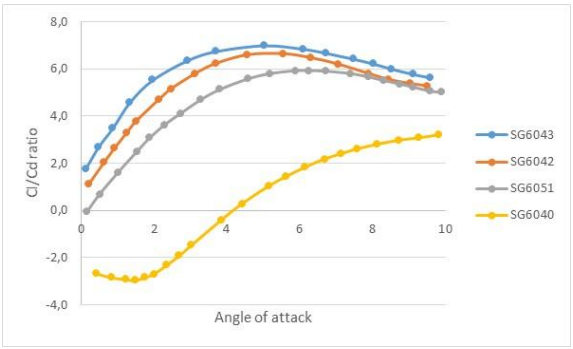

Fig. 1. *C_l/C_d ratio with angle of attack α_A*

The blade profiles were designed as shown at Fig.2.

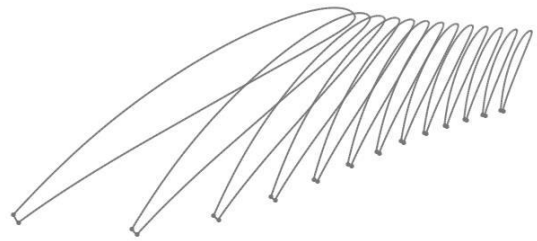

(a)

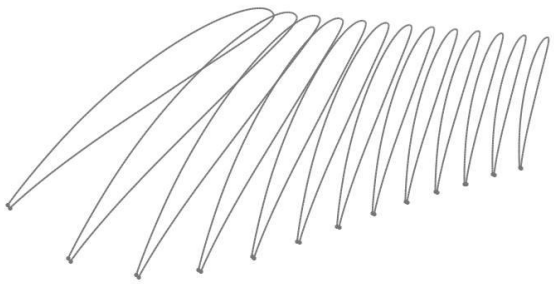

(b)

Fig. 2. *Blade profile distribution for Betz (a) and Schmitz (b) theory*

The commercial CAD program was used for modeling of both turbine geometries. The Betz and Schmitz wind turbine runner models are shown at Fig. 3.

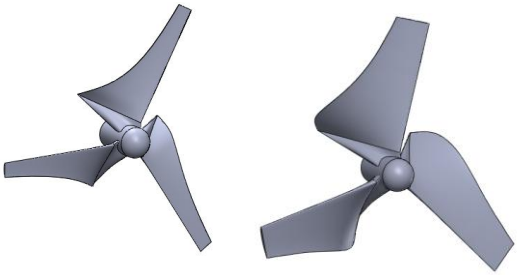

***Fig. 3**. Wind turbine runners according to Betz and Schmitz theory*

3. Numerical simulation

Operating characteristics of wind turbines were simulated using ANSYS- CFX. The simulation was set using Flow driven rigid body approach, where different prescribed mechanical torque values simulated the generator's electric load.

The used governing equations were based on the conservation form of the Reynolds averaged Navier-Stokes (RANS) equations system. The first equation is continuity equation, which can be written as:

$$\frac{\partial}{\partial t}\rho + \frac{\partial}{\partial x_i}(\rho \overline{u_i}) = 0$$

The second equation presents the equation for conservation of momentum:

$$\frac{\partial}{\partial t}(\rho \overline{u_i}) + \frac{\partial}{\partial x_j}(\rho \overline{u_i}\overline{u_j}) = -\frac{\partial}{\partial x_i}p + \frac{\partial}{\partial x_j}\left[(\mu + \mu_t)\left(\frac{\partial \overline{u_i}}{\partial x_j} + \frac{\partial \overline{u_j}}{\partial x_i} - \frac{2}{3}\delta_{ij}\frac{\partial \overline{u_k}}{\partial x_k}\right)\right]$$

where p denotes the pressure, u is the velocity, μ and μ_t are laminar and turbulent viscosity and δ_{ij} is the Kronecker delta function. Numerical modeling of turbulent flow is very complex process in which turbulence model play a significant role. It is used for calculation of fluctuating part of pressure and velocity in RANS equations. The appropriate turbulence model must be applied in order to accurately predict cavitation inception and detachment of the cavity from solid surface. In present study, the standard $k-\varepsilon$ model was used. It is a two-equation model which includes two extra transport equations which represent the turbulent properties of the flow.

$$\frac{\partial}{\partial t}(k) + \frac{\partial}{\partial x_i}(k\overline{u_i}) = \frac{\partial}{\partial x_j}\left[\left(\upsilon + \frac{\upsilon_t}{\sigma_k}\right)\frac{\partial k}{\partial x_j}\right] + P - \varepsilon$$

$$\frac{\partial}{\partial t}(\varepsilon) + \frac{\partial}{\partial x_i}(\varepsilon\overline{u_i}) = \frac{\partial}{\partial x_j}\left[\left(\upsilon + \frac{\mu_t}{\sigma_\varepsilon}\right)\frac{\partial \varepsilon}{\partial x_j}\right] + C_{1\varepsilon}\frac{\varepsilon}{k}P - C_{2\varepsilon}\frac{\varepsilon^2}{k}$$

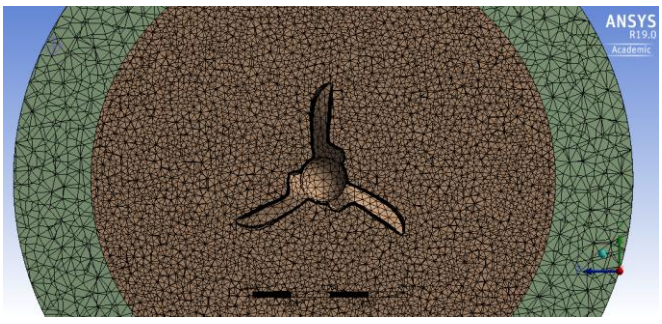

***Fig. 4**. Computational mesh*

The numerical domain was discretized by unstructured tetragonal mesh (Fig. 4). Grid dependence study was made using Richardson's extrapolation where three meshes with different mesh densities were tested. The grid convergence index presenting the calculated uncertainty was less than 5% for fine mesh and less than 7% for medium mesh. In order to assure minimal discretization error, the finest mesh with total number of 1714660 elements was used for numerical analysis.

Defining the right boundary conditions, it is a key to a successful numerical simulation. The boundary conditions in pipe, where turbine runners were mounted were prescribed as shown at Fig. 5 and detailed in table 1.

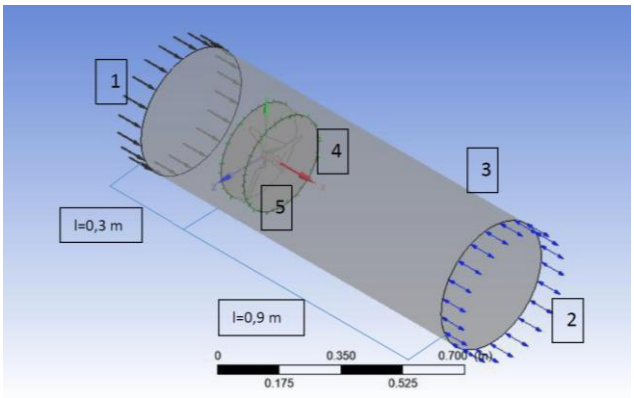

***Fig. 5**. Computational domain and boundary conditions*

***Table 1:** Boundary conditions.*

Number	Boundary condition type	Variable
1	Inlet	Velocity
2	Outlet	Pressure
3	Wall	Free slip
4	Rotor	Rotating, No slip
5	Interface	Frozen Rotor Stator

3. Experimental setup

The wind turbine runners were mounted into the inlet pipe of radial fan test section in laboratory. The wind was produced using frequency regulated electric motor which power the fan, as shown at Fig. 6.

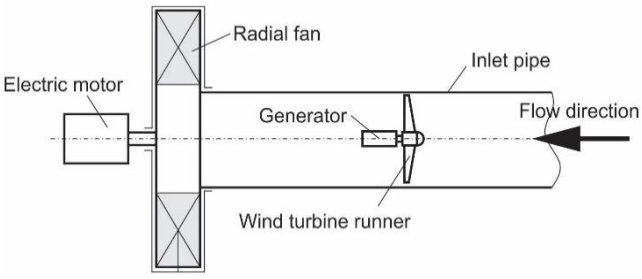

***Fig. 6**. Test section and turbine runner*

Wind turbine runners were directly connected to the axis of the generator. For the production of electrical energy, we used the permanent magnet brush DC motor, which operated in generator mode. The basic characteristics of motor are summarized in the table 2.

Table 2: *Generator characteristics.*

Maximal voltage	12 V at 4700 rpm
Nominal power	60W
Maximal allowed current	5,85 A
Torque constant	100 mN/A

The wiring diagram of generator is shown at Fig. 7. The induced voltage on generator equals

$$U_i = U_M + I_R\, R_R$$

Where mechanical power depends on torque and constant k_m as foloows

$$P = M\,\omega = (k_m\ \ I_R)\,\omega$$

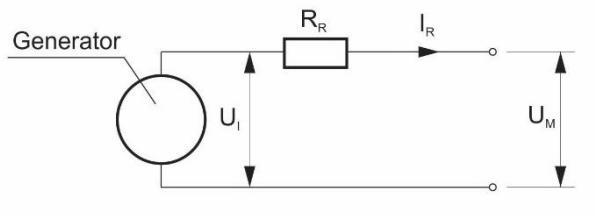

Fig. 7*. Wiring diagram*

National instruments 9401 module on 9171 carrier on was used for data acquisition. Optical encoder (5 V) was used for rotational speed measurements.

4. Results

4.1. Numerical simulation results

We performed numerical simulations of the wind turbines using both geometries and two different wind speeds. The simulations we performed were transient. The angular velocity of rotor was zero at the simulation start. The simulations were stopped at the moment when rotor angular velocity become constant. In the continuation results will be presented for the case of wind velocity 16 m/s.

Fig. 8 shows operating characteristics for Betz geometry at 16 m/s wind speed. We used normalized values of power, which means that the power value is divided by the maximal power value. This allows us to present results in values between 0 and 1, where value 1 stands for best efficiency.

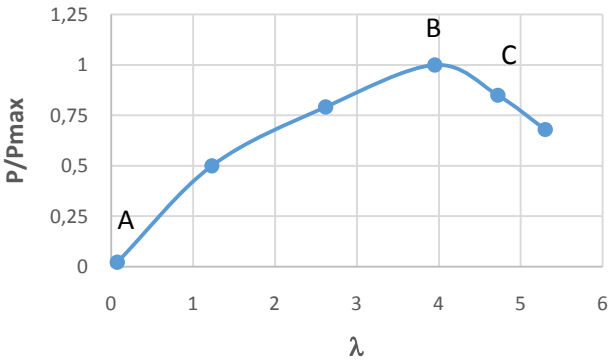

Fig. 8*. Operationg charateristics of Betz geometry at 16 m/s wind speed*

CFD enables detailed analysis of flow variables and give us deeper insight of flow characteristics of machinery Fig. 9 shows velocity field and velocity vectors for Betz turbine at 16 m/s. The point A represents a velocity field for lowest velocity ratio λ. As we can see from the figure, the flow separation occurs in the point A. On the other hand, we have points B and C, which both have higher efficiency, and their velocity fields do not differ that much.

Fig. 10 shows operating characteristics for Schmitz geometry at 16 m/s wind speed. It is evident that characteristics show same trend comparing to Betz turbine characteristics shown at Fig. 8. The difference is at optimal value λ_{opt} which is $\lambda_{opt,Schmitz}$=3,3 and $\lambda_{opt,Betz}$=3,9. The reason for this is in different geometry of runners.

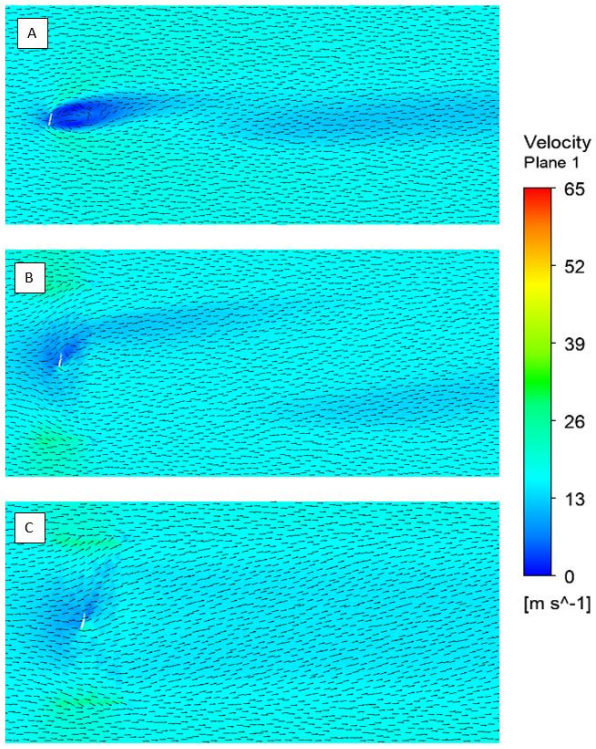

Fig. 9*. Velocity field for Betz turbine geometry at 16 m/s wind speed*

The velocity field and velocity vectors for Schmitz turbine are shown on Fig. 11. As it follows from diagram, similar nature as presented for the case of Betz turbine can be concluded.

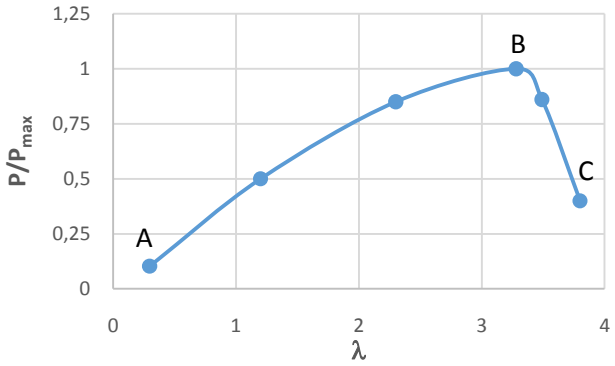

Fig. 10*. Operating characteristics of Schmitz geometry at 16 m/s wind speed*

4.2. Experiment results

The measurement of operating characteristics was performed for both wind turbine runners. The "wind" velocity was increased using frequency regulated electric motor. The Fig. 12 show the turbine runner rotating frequency for different wind speeds and mechanical power measured with the DAQ system.

It is evident, that turbine rotating frequency achieved more than 6000 rpm or 100 Hz at the wind speed of 10 m/s. At this operating point, mechanical power of system equals $P = 20\ W$.

Since both turbine runners were 3D printed from PLA filament, wind velocity was not increased further due to the mechanical

properties (strength of material) limitation. According to this, operating measured characteristics did not achieve the peak as shown at Figs. 8 and 10, where velocity boundary condition was set to the value of 16 m/s.

5. Discusion and conclusions

The CFD results presented clearly show, that wind turbines have to be precisely designed for the area of operation. As we can see the performance of the wind turbine rotor begins to increase, up to the point where it reaches its peak at λ_{opt}. This peak represents the optimal operating point of the wind turbine. Past its peak, the performance begins to deteriorate.

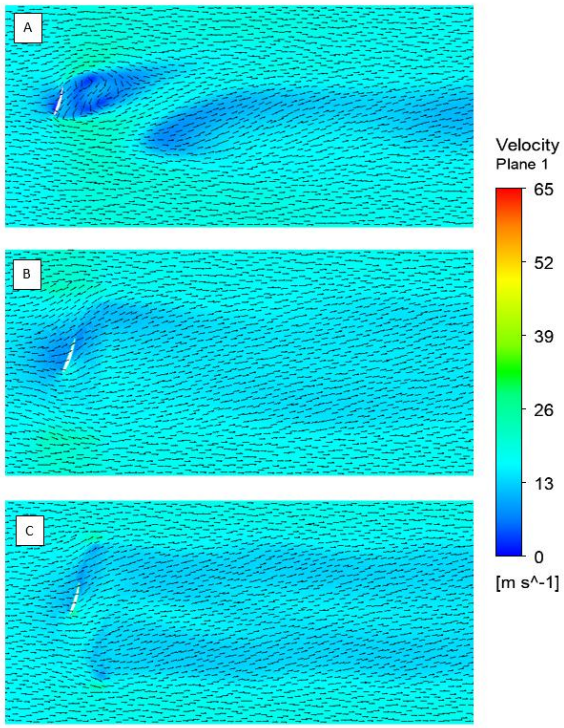

***Fig. 11**. Velocity field for Schmitz turbine geometry at 16 m/s wind speed*

The quantitative analysis of CFD results show that geometry according to the Schmitz theory performs a lot better. The difference was more evident at wind of 16 m/s, where the power output of the Schmitz geometry is 38.5W, while the Betz geometry only produces 14.8W. On the other hand, we have the 8 m/s wind where both geometries performed poorly, but still the Schmitz geometry output was 4,7W, while the Betz geometry produced only around 2,3W.

The reason for better characteristics of Schmitz runner geometry is in surface area of runner. If we look at Fig. 3 we see that the Schmitz geometry has a much larger surface area comparing to the Betz geometry, which helps to extract more energy from the wind.

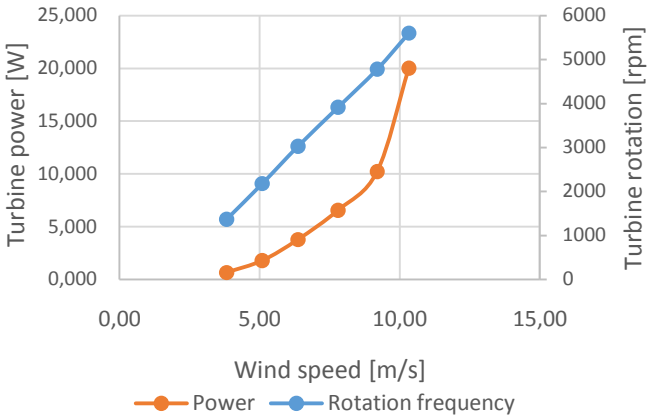

***Fig. 12**. Measurement of operating characteristics for Schmitz turbine*

The experimental analysis showed that used electric generator characteristics and analyzed runners are not compatible for the case of runners printed of PLA. To perform complete characteristics measurement, the generator should be optimized or runner's material should be replaced with more rigid one.

In conclusion, we see that Schmitz geometry is more suitable, because it produces twice as much power.

6. References

[1] W. Musial and B. Ram, "Large-Scale Offshore Wind Power in the United States," U.S. National Renewable Energy Laboratory, September 2010.

[2] Janič, "Design of geometry and numerical simulation of the operating charateristics of the rotor of the air turbine," University of Maribor, 2018.

[3] W. Musial and B. Ram, "Large-Scale Offshore Wind Power in the United States," U.S. National Renewable Energy Laboratory, September 2010.

[4] A. Janič, "Design of geometry and numerical simulation of the operating charateristics of the rotor of the air turbine," University of Maribor, 2018.

[5] M. Ragheb. "Optimal rotor tip speed ratio." 2014 Available: *http://mragheb.com/NPRE%20475%20Wind%20Power%20Systems/Optimal%20Rotor%20Tip%20Speed%20Ratio.pdf.*

[6] R. Gasch, J. Twele, "Wind Power Plants: Fundamentals, Design, Construction and Operation, second edition," Berlin, 2012.

[7] A. Hribernik, "Obnovljivi viri energije," Fakulteta za stojništvo, Maribor, 2012.

[8] H. Shah, N. Bhattarai, S. Mathew, C. M. Lim, "Low Reynolds Number Airfoil for Small Horizontal Axis Wind Turbine Blades, Sustainable Future Energy 2012 And 10th See Forum, 2012.